An Idealized Model of the World Ocean. Part I: The Global-Scale Water Masses

MICHAEL D. COX*

Geophysical Fluid Dynamics Laboratory/NOAA, Princeton University, Princeton, New Jersey

(Manuscript received 31 March 1989, in final form 26 June 1989)

ABSTRACT

A primitive equation, three-dimensional numerical model of the ocean, employing idealized versions of the real topography and surface boundary conditions, is used to study the water mass structure of the World Ocean. In particular, the response of the model to three fundamental changes in boundary conditions is investigated in an attempt to identify the mechanisms in the model which are responsible for the establishment of the largest scale features of the global water-mass structure. With the Drake Passage closed, thermohaline driving alone, and a fresh North Atlantic surface salinity specified, only the coarsest aspects of the observed T and S structure are reproduced and the entire World Ocean below the thermocline is dominated by water formed at the southern boundary. The salinity configuration in particular, lacks much of its observed structure in this case. When the Drake Passage is opened, the resulting circumpolar flow serves to isolate the extreme southern ocean. This allows waters of northern and midlatitude origin to invade the subthermocline zones, producing the familiar tongues of fresh water at intermediate depths. Wind driving further isolates the extreme Southern Ocean and improves the shape and positioning of the fresh water lenses, particularly in the Southern Ocean. Finally, increasing the salinity of water formed at the surface of the northern Atlantic produces distinct salinity maxima in the deep water throughout the World Ocean, bringing the overall salinity structure into broad agreement with observations. Passive tracers are used to establish water mass origins.

1. Introduction

The configuration of the largest scales of the temperature and salinity structure within the World Ocean has been well documented in recent decades. Considerable effort, both in observational analysis and theoretical modeling, has been expended toward the understanding of the known state of the ocean, and much progress has been achieved. There remain, however, some very fundamental uncertainties about why the water masses are configured as they are. Probably due to its higher degree of complexity, interpretation of the known salinity structure has proven more difficult than that of temperature. As an example, Worthington (1981), in analyzing a census of the T and S observations in the World Ocean, questions why the deep water occupying the North Pacific is fresher than the Antarctic Circumpolar water which is presumably its source. Is it a remnant of a former World Ocean which was significantly fresher? Or might it be produced by diapycnal mixing with fresher waters lying above?

This and many other such questions about the known salinity (and temperature) structure are difficult to address considering the observations alone. Theoretical models present an opportunity to extend our understanding in such cases. They, in their more complete forms however, approach the complexity of the real ocean and can be equally as difficult to interpret if the appropriate fundamental analysis of the solutions they generate is not performed.

The objective of the present series of studies is to carry out, at least in part, such an analysis of the very largest scale water masses and circulation regimes occurring within the World Ocean as represented in an idealized, numerical model. This study, part 1, will concentrate on the origin of the major water masses occurring in the model. A subsequent study, part 2, will address the corresponding circulation patterns.

Observational studies, while benefitting greatly in recent years from advances in hydrographic and current measuring technology, have been, for obvious reasons, restricted to less than global scales. However, the judicious combination of nonsynoptic observations from various separate studies has been used to infer interbasin patterns of flow that are proving helpful in understanding the global circulation. An example of such a study is that of Reid and Lynn (1971) linking the deep-water formation areas of the North and South Atlantic with the deep Indian and Pacific oceans. Gordon (1986) has identified a closed global-scale circulation regime describing the supply and replenishment of North Atlantic Deep Water to the World Ocean. Warren (1981) provides an excellent overview of the circulation of the deep ocean on a global scale.

The analysis of the spread of natural and anthropogenic tracers within the oceans has also contributed

* Michael Cox died 10 September 1989 after a long illness. Correspondence should be addressed to Dr. Kirk Bryan, Geophysical Fluid Dynamics Laboratory, Princeton University, P.O. Box 308, Princeton, NJ 08542.

greatly to our understanding of the formation of the global-scale water masses. As an example, Bolin and Stommel (1961) used ^{14}C observations in combination with T and S measurements to establish a quantitative estimate of the ratio of Antarctic Bottom Water, North Atlantic Deep Water and Intermediate Water which go to make up the bottom water of the Pacific and Indian oceans. Broecker, Takahashi and Takahashi (1985) expand upon this work by considering the more conservative tracer, initial phosphate, and show that water formed at the surface in lower latitudes must also be considered an end member in the process of deep-water formation.

The modern study of large-scale oceanic water masses and circulation using analytical models, beginning with the foundational works of Sverdrup, Stommel and others nearly four decades ago, has tended to focus primarily upon wind-driven solutions, and has been typically limited to domains of single ocean basin scale. This has been true largely because of the more tractable nature of the linear equations which are solved in analytical wind-driven models, and the simpler boundary conditions associated with rectangular domains. The thermohaline component of the general circulation has proven much more difficult to handle analytically due to the nonlinear nature of the fundamentally important convective processes which drive the thermohaline cells. Probably the best known exception to the limitations of these models is the work of Stommel and Arons (1960) who described a simple but elegant model for deep flow in the ocean. Kuo and Veronis (1973) demonstrated the application of this basic model to an idealized version of the geometry of the World Ocean.

Numerical modeling studies are generally not as hampered by the existence of strong nonlinear processes, and are more easily applied to domains of irregular shape and multiple connectedness. However, they have also typically focussed on single basin solutions, with wind considered the primary or only driving force. This has occurred, in some part, due to a need for historical continuity with the previous analytical work. Also, these solutions are simply less costly to obtain than buoyancy driven or multiply connected regimes which generally require longer integration times to reach a steady state. Exceptions are found in a series of World Ocean modeling studies summarized by Bryan (1979). These studies, due to their costliness, have tended to be composed of single experiments which are analyzed in terms of accuracy in simulation of what is known of the real ocean. While they have contributed significantly to our understanding, much more work is needed to establish how and why these models generate the particular solutions they do.

More recently, advances in computer technology have enabled numerical investigators to resolve mesoscale eddies explicitly, even using the full, primitive equation models. However, these integrations can typically be carried out for only several decades of ocean time at most and significant long-term drifts usually remain in the deep water components of the solutions. While they are proving to be valuable in the study of flow above the thermocline, uncertainty arising from incomplete convergence below the thermocline renders them less useful for the study of the deep ocean.

The robust diagnostic technique, in which observed data is inserted into the deep ocean, can be used to shorten the convergence time scale of the model. However, although the density structure is held close to that of the real ocean in this case, experience has shown that the resulting circulation patterns can be unrealistic and misleading. Toggweiler et al. (1989), for example, find that simulations of ^{14}C in a robust diagnostic model of the World Ocean are much inferior to those produced by an equivalent prognostic model, even though the accompanying temperature and salinity patterns of the former are superior. They attribute this to the relatively poor job the robust diagnostic model does in reproducing the current structure. Deep water masses are normally formed at high latitudes by interaction with the atmosphere and then sink. In the robust diagnostic model, they tend to be formed locally through the artificial Newtonian damping term. Vertical motion throughout the deep water is seriously distorted by this surrogate process. Also, the imposition of known water masses upon a model a priori fundamentally limits the capacity of the model for the study of their formation.

An alterative approach for the study of the subthermocline ocean is to utilize the power of the modern supercomputer not in terms of additional resolution but in terms of longer integration times, enabling the investigator to achieve solutions which are in true balance in the deep ocean with respect to the physics of the numerical model used. The ultimate ocean model would, of course, be one combining eddy resolution with practicable integration times of the multiple centuries needed to achieve a steady state solution below the thermocline. Even with today's rapidly advancing parallel-computing technology, such a model is probably still more than a decade into the future.

Meanwhile, based upon previous experience with each of the modeling approaches discussed above (eddy-resolving, robust diagnostic and long-term non-eddy resolving), it appears that the non-eddy resolving aspect of the latter is arguably less damaging to the integrity of the solutions obtained for the subthermocline ocean than the limitations discussed above for the other two. For this series of investigations, a model of the World Ocean, incorporating idealized topography, has been constructed for the purpose of studying the largest scales of water mass structure and circulation within the global ocean. The gridspace resolution has been maximized to exercise the full capability of the modern supercomputer in integrating the several thousands of years necessary to achieve prognostic, steady state solutions. In the present study, Part 1, only

the water mass structure will be considered. Since the model has been idealized both in topography and boundary conditions, there will be less emphasis on simulation of the real ocean and more consideration placed upon simply what determines the particular characteristics of the water masses that the model generates. Of particular interest will be the response of the water mass structure to various fundamental changes in boundary conditions.

After a general description of the model in section 2, an important property of the Antarctic Circumpolar Current in controlling the relative rates of abyssal water production between the northern and southern oceans will be discussed in section 3, using a simple rectangular basin. The region of solution is then expanded to the World Ocean for the remainder of the study. A description of the four basic experiments upon which this study is based is provided in section 4, and in section 5 patterns of temperature and salinity of the experiments are analyzed. Idealized tracers are used in section 6 to analyze the origins of the water masses of the model, and in section 7 to analyze the exchange of water masses induced by the changes in boundary condition between the four experiments. Finally, a summary of the most significant results of the study is given in section 8.

2. Description of the model

The model used in this study is the multilevel numerical model described in Bryan (1969) and adapted to modern vectorizing computers by Cox (1984). The continuous equations will be given here. A detailed description of the finite difference formulation may be found in the references given above. The model is governed by the Navier–Stokes equations modified by the Boussinesq approximation and the hydrostatic assumption. Molecular viscosity in the horizontal plane is replaced by a term of Laplacian form. Let $m = \sec\phi$, $n = \sin\phi$, $u = a\dot{\lambda}m^{-1}$, and $v = a\dot{\phi}$, where a is the radius of the earth, ϕ the latitude, and λ the longitude. It is convenient to define the advection operator

$$\mathcal{L}(\mu) = ma^{-1}[(u\mu)_\lambda + (v\mu m^{-1})_\phi] + (w\mu)_z. \quad (1)$$

The equations of motion on a sphere are

$$u_t + \mathcal{L}(u) - 2\Omega nv = -ma^{-1}(P/\rho_0)_\lambda + F^\lambda, \quad (2)$$

$$v_t + \mathcal{L}(v) + 2\Omega nu = -a^{-1}(P/\rho_0)_\phi + F^\phi, \quad (3)$$

$$\mathcal{L}(1) = 0, \quad (4)$$

$$g\rho = -P_z, \quad (5)$$

where ρ_0 is unity in cgs units. The conservation equations for the potential temperature, salinity and passive tracers respectively are written

$$T_t + \mathcal{L}(T) = F^T \quad (6)$$

$$S_t + \mathcal{L}(S) = F^S \quad (7)$$

$$\mathrm{Tr}_t + \mathcal{L}(\mathrm{Tr}) = F^{\mathrm{Tr}}. \quad (8)$$

The equation of state $\rho = (T, S, z)$ is calculated from a nine-term polynomial fit to the Knudsen formula for each vertical level (Bryan and Cox 1972). The terms in F represent the effects of turbulent viscosity and diffusion. Let

$$\Delta\mu = m^2\mu_{\lambda\lambda} + m(\mu_\phi m^{-1})_\phi, \quad (9)$$

then

$$F^\lambda = A_{MV}u_{zz} + (A_{MH}a^{-2})\Delta u, \quad (10)$$

$$F^\phi = A_{MV}v_{zz} + (A_{MH}a^{-2})\Delta v, \quad (11)$$

$$F^T = [(A_{HV}\delta^{-1})T_z]_z + (A_{HH}a^{-2})\Delta T + \gamma(T^* - T), \quad (12)$$

$$F^S = [(A_{HV}\delta^{-1})S_z]_z + (A_{HH}a^{-2})\Delta S + \gamma(S^* - S), \quad (13)$$

$$F^{\mathrm{Tr}} = [(A_{HV}\delta^{-1})\,\mathrm{Tr}_z]_z + (A_{HH}a^{-2})\Delta\,\mathrm{Tr} + \gamma(\mathrm{Tr}^* - \mathrm{Tr}), \quad (14)$$

$$\delta = \begin{cases} 1, & \text{statically stable} \\ 0, & \text{statically unstable} \end{cases} \quad (15)$$

$$\left.\begin{aligned} w = T_z = S_z = \mathrm{Tr}_z = 0 \\ \rho_0 A_{MV}(u_z, v_z) = \tau^\lambda, \tau^\phi \end{aligned}\right\} \quad Z = 0, \quad (16)$$

$$\left.\begin{aligned} w = T_z = S_z = \mathrm{Tr}_z = 0 \\ \rho_0 A_{MV}(u_z, v_z) = \tau^{\lambda b}, \tau^{\phi b} \end{aligned}\right\} \quad Z = -H, \quad (17)$$

where A_{ab} is the mixing coefficient corresponding to

$$a = \begin{cases} M, & \text{momentum} \\ H, & \text{heat, salinity or tracer,} \end{cases}$$

$$b = \begin{cases} V, & \text{vertical} \\ H, & \text{horizontal.} \end{cases}$$

The quantities τ^λ, τ^ϕ are the respective surface stress components, and at the bottom a quadratic drag law is used where

$$\tau^{\lambda b}, \tau^{\phi b} = \rho_0 c_0 (u^2 + v^2)^{1/2}(u\cos\alpha - v\cos\alpha, \; u\sin\alpha + v\cos\alpha)$$

$$c_0 = 1.3 \times 10^{-3}, \quad \alpha = -10^0: \phi > 0,$$

$$\alpha = 10^0: \phi < 0.$$

Both velocity components and the normal gradient of temperature, salinity and passive tracers are zero at all lateral boundaries. The final term in Eqs. (12)–(14) is a Newtonian damping facilitating the flux of heat, salt and passive tracer through the surface of the model. The coefficient γ is taken to be 1/(100 days) for potential temperature and passive tracers, and 1/(400 days) for salinity, in the top level of the model. It is set to zero for all variables below the surface level. The

mixing coefficients have been set to $A_{HH} = 1 \times 10^7$ cm^2 s^{-1}, $A_{MH} = 4 \times 10^8$ cm^2 s^{-1}, $A_{HV} = 0.5$ cm^2 s^{-1}, $A_{MV} = 50$ cm^2 s^{-1}. The latter quantity is somewhat large, but is necessary to suppress vertical gridpoint noise in equatorial regions.

The region considered in this study is the idealized approximation of the real topography of the World Ocean shown in Fig. 1. In its simplification of the topography, it is reminiscent of the configuration used by Kuo and Veronis (1973) in their application of the Stommel and Arons deep circulation model. The present rendition is somewhat more detailed by the inclusion of a separate land mass for both Australia and New Zealand. Horizontally, the resolution is constant throughout the grid at 2 degrees meridionally by 2.5 degrees zonally. Vertically, there are 12 levels covering the total depth of 4000 meters, expanding in thickness from 80 meters at the surface to 572 meters at the bottom. A flat bottom is assumed everywhere with the following exceptions. Sills at a depth of 1552 meters (7 levels) are placed between New Zealand and Australia, and Australia and Asia. Also, except for Expt. 1 in which the Drake Passage is closed off, a sill is placed across it at a depth of 2406 meters (9 levels). Midocean ridges have been neglected in this study for purposes of simplicity. (Their effect can and should be investigated in future work.) The meridional boundaries have been positioned to approximate the equivalent effective boundaries in the real ocean. The Antarctic Ocean is given the most extreme boundary at 70°S, the North Atlantic the next most extreme at 60°N, and the North Pacific is bounded at 55°N.

Except as noted later in the description of the specific experiments which have been carried out in this study, the surface boundary conditions are given by the distributions shown in Fig. 2. T^*, S^*, and τ^λ are based crudely upon long-term mean observational data for temperature, salinity and wind stress at the surface of the real ocean. The resultant distribution for sigma-theta arising from the given T^*, S^* is provided for reference. The meridional component of wind stress is set to zero for all experiments of this study.

Initial conditions for each experiment consist of basinwide homogeneity in both temperature (7°), salinity (34.7 ppt) and passive tracer (zero), and complete rest. The operational objective in carrying out the experiments is to generate solutions to the applied surface boundary conditions which are in complete steady state for all regions of the model ocean, including the deepest water. The centuries long duration of such integrations requires formidable computational efforts, even when applied to grids of only moderate resolution. The semi-implicit treatment of the Coriolis term, described by Bryan (1969), is used here to permit longer timestepping. In addition, when seeking a steady state solution, the useful technique of split timestepping (Bryan 1984) is available to decrease the computational load.

Using this method, the timestep applied to the state variables (T, S) may be lengthened appreciably so long as the timestep applied to the momentum is decreased in proportion. This enables one to overstep the otherwise limiting Courant-Friedrichs-Levy condition associated with the propagation of internal gravity waves in the model. In the steady state, length of timestep drops out of the equations so that the final solution is unchanged by this technique.

For the present model, an advantage of approximately 2.5 in speed is realized using this method. In addition, the timestep applied to the state variables may actually be further lengthened in the deep water where advective velocities are small. Using this technique, an additional acceleration factor of 15 is realized. The two time accelerations taken together yield a factor approaching 40 in convergence rate for the deepest regions of the model ocean. Since it is in these regions that the solution takes the longest to reach equilibrium, such a speedup is very useful in obtaining the type of solution sought here.

3. A fundamental property of the ACC

Before going on to study the solutions obtained in the model containing idealized global geometry, it will be useful to identify a fundamental role which the Ant-

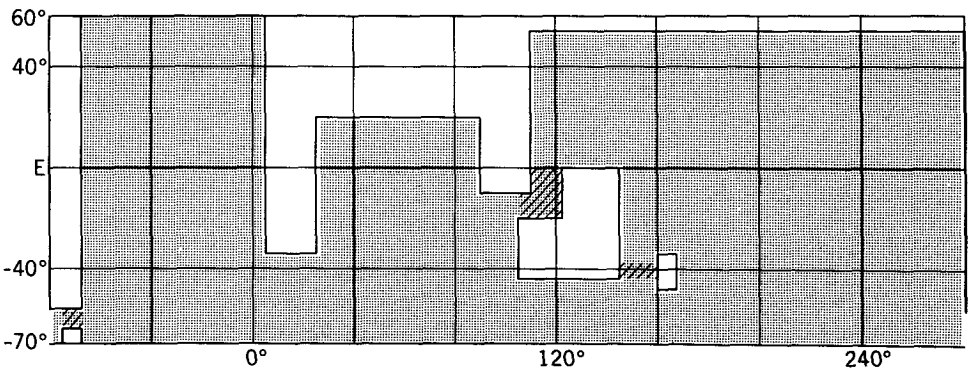

FIG. 1. The region covered by the model. The hatched areas designate sills described in the text. There is cyclic continuity from the right to left margin.

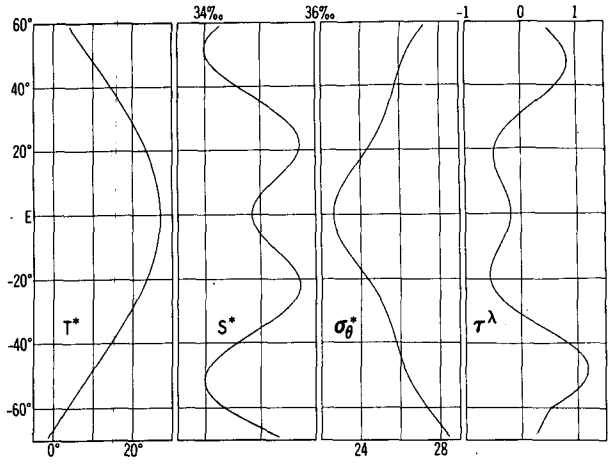

FIG. 2. Surface boundary conditions of the model. Sigma-theta is calculated directly from T^* and S^*. The wind stress is given in units of dyn cm^{-2}.

arctic Circumpolar Current (ACC) plays in controlling the relative rate of deep and bottom water formation between the Northern and Southern hemispheres. It is reasonable to expect that a mutually limiting relationship will exist between the various potential poleward sources of surface derived deep and bottom waters. Suppose water of a certain density is being produced vigorously in the deep southern ocean and is free to move laterally into the deep northern ocean. If there is little or no source at the surface of the northern ocean for water of this great density, then the southern ocean will dominate deep-water production for the entire system.

This phenomenon was illustrated quite simply by the study of Bryan (1986). In this work, an equatorially symmetric, two hemisphere numerical model, was used to study the interaction between the global-scale thermohaline circulation and the surface-induced salinity distribution. It was found that, under conditions of completely symmetric surface forcing, production of abyssal waters in such a regime will be divided equally between the two polar boundary regions of the model. However, when a temporary perturbation increasing surface salinity was applied to one hemisphere, it was found that the abyssal water production could be induced to move totally and permanently to that hemisphere. Abyssal water production was then cut off completely from the other hemisphere.

This is an extreme illustration of how the various deep and bottom water production regions of the World Ocean need to be in adjustment to each other. A further controlling factor in determining deep water characteristics is the much longer time scale, eddy diffusion of heat vertically through the thermocline in middle and low latitudes. This process may be thought of as a sink of high density water just as the poleward, convection dominated regions discussed above are sources of it. In the real world, a balance has been established between these various controlling factors such that the deep and bottom waters of the global ocean take on water mass characteristics in corresponding proportion.

The Antarctic Circumpolar Current may be expected to play a significant role in the balance described above. In its position just to the north of the expected deep convection regions of the Southern Ocean, what effect does it have in altering the balance of production of global subthermocline water, particularly relative to northern production areas? Some help is provided by the study of Gill and Bryan (1971) in which a series of numerical experiments was conducted to investigate the role of the ACC in the circulation of the Southern Ocean. They carried out integrations both with and without a cyclic gap across the southern end of their model box, studying the effects of the presence and absence of a southern throughflow on the circulations produced. Unfortunately, their model extended only to the equator, so interactions with a Northern Hemisphere were not present. However, among their other results was the very interesting finding that the presence of the gap, and the ensuing ACC, resulted in a significant warming of the steady state abyssal waters to the north of the ACC. They attributed this to the fact that, since the ACC is in geostrophic balance, there must be a meridional density gradient present across it. This produces a density barrier effect across the ACC in which the higher densities of the extreme Southern Ocean are, to some degree, isolated from those north of the ACC. Since the density at the southern wall is determined strongly by the surface boundary condition whether the ACC is present or not, the density to the north of the ACC must be reduced as a result of its presence.

Such an isolating effect has strong implications for the subthermocline water production of the Southern Ocean relative to any competing northern source. How would Northern Hemisphere deep-water production have been affected by the presence or absence of the ACC in the Gill and Bryan study had a Northern Hemisphere been present in their model? To study this question, a box model similar to theirs has been constructed, except that a Northern Hemisphere ocean has been added with a potential source of deep water provided at the northern wall by the imposed surface boundary condition. The region of the model is taken to be the rectangular box overlying the Atlantic sector of Fig. 1, formed by extending the theoretical west African boundary at 5°E longitude to the southern wall. The surface thermohaline forcing is T^*, S^* of Fig. 2. Wind is set to zero for this test. Note that Gill and Bryan (1971) find the ACC to be primarily driven not by wind, but by a surface buoyancy flux induced pressure difference across the topographic sill in their model. Two cases have been run, one without a topographic gap across the Southern Ocean, and one with a gap interrupting the meridional walls as noted in Fig.

1, and extending through 9 of the 12 model layers, or 2406 of the 4000 meter total depth. Both models were run in split time, accelerated mode for a total of 108 years of surface time and 1620 years of bottom time. Vertical acceleration was then removed and the runs were advanced another 18 years to verify that steady solutions had been obtained. The following discussion is based upon these solutions.

The influence of the southern throughflow upon the mass properties of the solution is shown in Figs. 3 and 4 where temperature and salinity are depicted for each of the two cases. In agreement with the Gill and Bryan results, the temperature of the subthermocline waters is increased significantly in the case with a gap. The increased meridional density gradient across the latitude of the gap, as in their case, is needed to maintain the stronger zonal jet produced by the gap throughflow.

Since buoyancy flux by salinity effects (S^*) is more structured meridionally than is temperature, the resulting patterns of salinity, shown in Fig. 4, are also somewhat more revealing, particularly of the flow patterns at intermediate depths in the two cases. The influence of the high salinity surface waters prescribed at the southern wall is seen to decrease in the deep interior in the presence of the throughflow, consistent with the thermal effects noted above. However, equally interesting is an accompanying amplification of the low salinity tongue originating from the surface salinity boundary condition at the northern wall and penetrating southward at intermediate depths. This may be considered an analogy to North Atlantic Deep Water in the real ocean, even though the salinity signature is of opposite sign. Its larger amplitude in the case with a gap indicates the controlling influence the ACC has over the production of deep water in northern regions of the model.

The meridional and vertical components of the mean flow are shown as a meridional mass transport

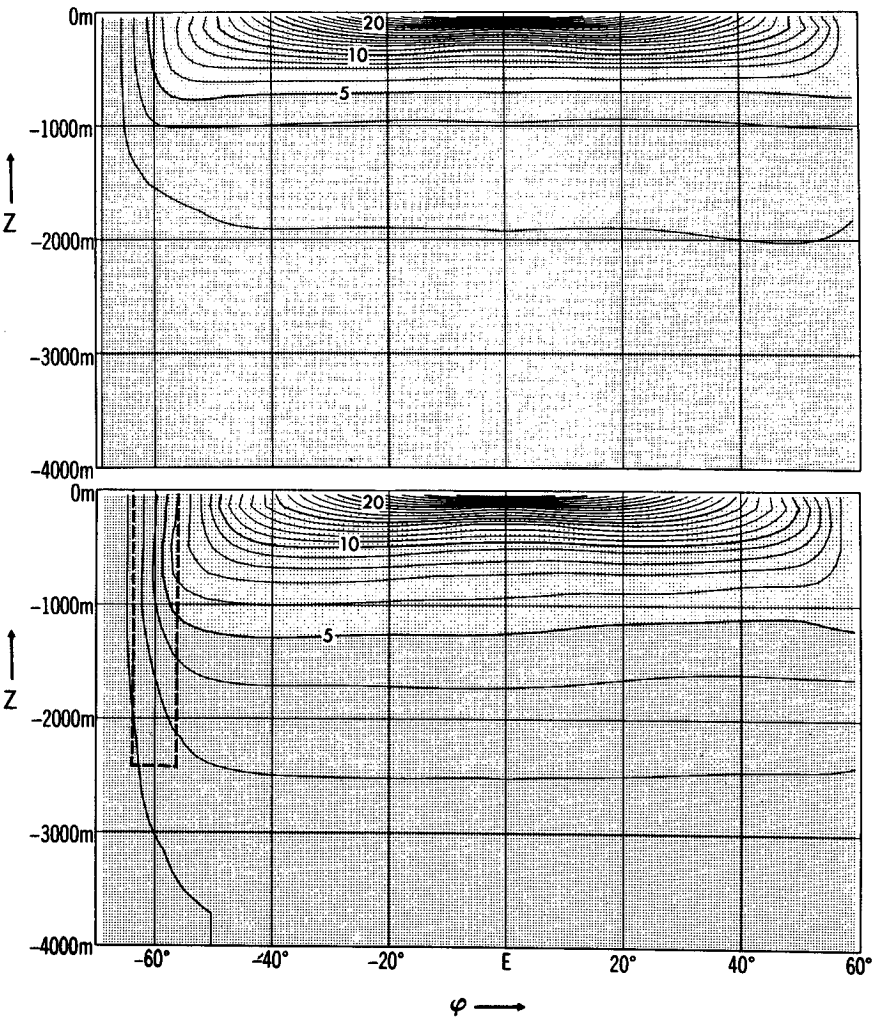

FIG. 3. Zonally averaged temperature in the single basin experiments with no gap (top), and with a tap (bottom) as designated by the dashed line.

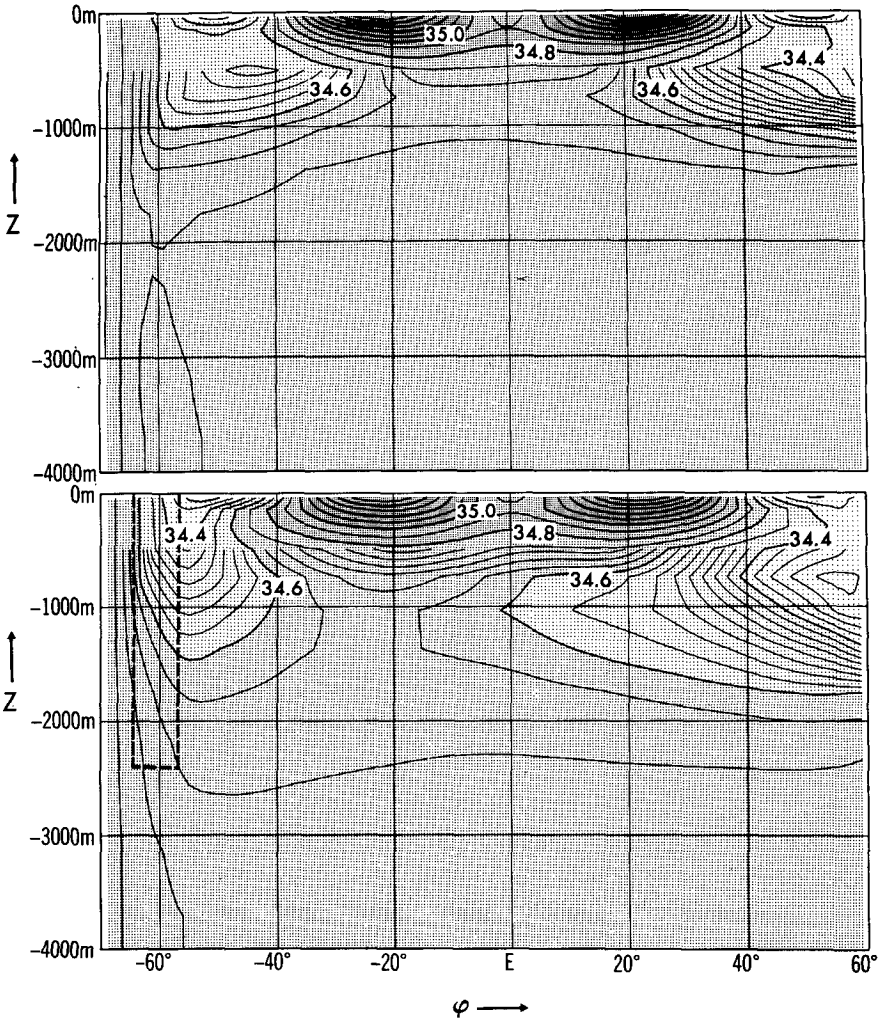

FIG. 4. As in Fig. 3, but for zonally averaged salinity.

streamfunction in the panels of Fig. 5 for the two cases. In the top panel, representing the non-gap case, a strong overturning cell extending well into high northern latitudes indicates dominance by the Southern Ocean in deep water production. Only a small, shallow cell exists in the north representing subsurface water production there. However, when the gap is opened, the relative dominance of the Southern Ocean is significantly reduced. The amplitude of the southern cell is decreased by a factor of five or more. At the same time, the influence of subsurface water production in the north increases, the meridional cell there increasing by more than two and deepening. As in the case of Gill and Bryan (1971), the gap acts as a southern boundary for the southern cell since, as they have shown, mean geostrophic meridional flow cannot be maintained in the absence of meridional boundaries. South of the gap, the direction of the overturning cell reverses. The significance of this response is unclear but will be addressed in Part 2 of this study.

In summary, the presence of a cyclic southern throughflow causes a partial isolation of the ocean to the south of it. It may be expected that the stronger the throughflow, the more isolated the ocean to the south will be. The resulting decrease in density of the water passing from the Southern Ocean production areas northward in the deep ocean allows the northern deep or intermediate water production areas to be more competitive, and they strengthen accordingly. Thus, the strength of the ACC may be expected to have a distinct influence on, say, the production of North Atlantic Deep Water.

4. The four experiments

The objective of the present series of studies is to carry out an analysis of the largest scale water masses and circulation regimes occurring within the World Ocean as represented in the idealized numerical model. In particular, it would be useful to identify, if possible,

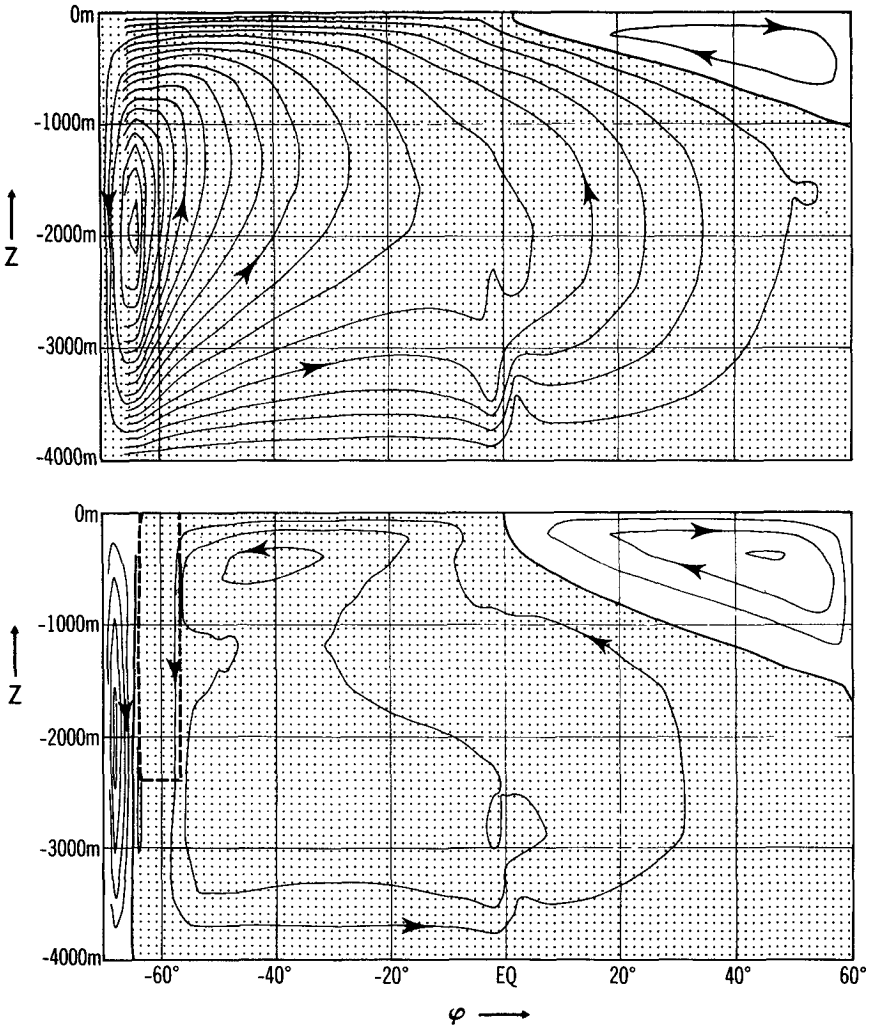

FIG. 5. Meridional mass transport streamfunction in the single basin experiments with no gap (top), and with a gap (bottom) as designated by the dashed line. Each contour represents 2×10^6 $m^3 s^{-1}$ of flow.

the most fundamental mechanisms within the model which control these attributes. Toward this end, a set of four experiments has been designed to study the response of the model to very basic changes in boundary conditions. Clearly, the choice of these four must be considered, to some degree, arbitrary since there are a myriad of such experiments that could be carried out, changing not only boundary conditions, but mixing coefficients, internal physics, etc. However the present four have been chosen to maximize the likely yield in terms of understanding which is most needed at our current position in World Ocean modeling.

Experiments 1 and 2 are an expansion of the two single basin experiments of the previous section. The topography is simply extended to the idealized World Ocean topography of Fig. 1. Both are driven solely by thermohaline forcing at the surface; T^*, S^* of Fig. 2 are applied at all longitudes and the wind stress is set to zero. The only difference between the two experiments is that the small hatched area of Fig. 1, representing the Drake Passage, is filled with land in Expt. 1, and opened to 2406 meters depth in Expt. 2. The questions these two experiments address are twofold. First, how much of the elementary structure of the water masses of the World Ocean can be reproduced with a thermohaline driven model in the absence of direct wind driving? Second, does the presence or absence of the ACC in the model affect each of the three basins of the idealized model equally and in the same manner as described in the previous section for the single basin, or is there significant basin-to-basin variation in response?

Experiment 3 is a duplication of Expt. 2 with the addition of the zonal wind stress of Fig. 2 applied at

all longitudes. Its broad purpose is to determine what component of the water mass structure is sensitive to, or relies upon, direct wind driving.

Although the surface salinity distribution of Fig. 2 is a reasonable approximation to the world zonally averaged surface salinity based upon observations, there is considerable longitudinal variation in surface salinity around the world. In particular, the surface salinity of the northern North Atlantic is considerably greater than that at similar latitudes of the North Pacific. The final experiment of the present series has been designed to study the sensitivity of the model solution to the application of a simple Atlantic/Pacific contrast in northern surface salinities based crudely upon those observed. Experiment 4 is a duplication of Expt. 3, including an alteration to the boundary condition for salinity as described below.

To the final term of Eq. (13) is added an additional Newtonian term of identical structure with a reference salinity, $S^{*\prime}$, of 36.5 ppt, a spring constant, γ', of 1/(25 days), and effective only over an array of nine grid boxes positioned along the eastern boundary of the Atlantic sector between 32° and 38°N, and between the surface and 384 meters depth (three levels). This array is chosen to approximate the position of the saline Mediterranean outflow in the real ocean. The reliance on a single source for saline water in this manner is clearly an oversimplification of the real water flux processes in the North Atlantic. However, the parameters above were found empirically to yield a salinity within the resulting deep water of the model North Atlantic which agrees broadly with observations. The purpose of this experiment is to investigate the response of the water mass structure of the remainder of the World Ocean to the production of high salinity water in the deep North Atlantic.

Each of the four experiments was initialized to the homogeneous conditions described earlier and integrated to a steady state in the split timestep, accelerated mode. The temperature and salinity at selected local points within the interiors of the three basins of the model were monitored to judge the convergence of the solution. Each of the four experiments was integrated a total of 234 years of surface time and 3510 years of bottom time, although the solutions were essentially steady during much of the last half of this period. It is worthwhile noting, however, that significant adjustments were still occurring the deeper waters between years 1000 and 2000 of the integration there. An additional integration of 18 years was carried out at the end of each experiment, in which vertical timestep acceleration was removed, to insure that the split timestepping had no effect upon the steady state solution.

5. Temperature and salinity patterns

A considerable amount of information is contained in the solutions which have been generated. It is a formidable task to display the three-dimensional water mass structure for each basin of the idealized model, for each of the four experiments, in any degree of completeness. A reasonable compromise may be achieved by presenting zonal mean, meridional–vertical sections for each of the three rectangular regions of the idealized model: the Atlantic, Indian, and Pacific basins. The largest scale properties of the major water masses of the World Ocean are revealed reasonably well in such sections. To provide a reference with which the solutions can be compared, the long-term mean, observational data of Levitus (1982) have been redrafted for each of the three basins in Fig. 6, for both temperature and salinity. These patterns and the water masses associated with them have been discussed extensively in the literature, leaving no need for further discussion here. We will instead, proceed directly with an analysis of the model solutions in broad comparison to the observed patterns. It should be reiterated at this point that, since the model used here has been highly idealized, lacking much of the observed structure of the topography and surface forcing of the real World Ocean, less emphasis will be placed in this analysis upon precision of simulation of the real ocean than upon the sensitivity of the model to the fundamental changes in boundary conditions represented in the four experiments. The objective is to determine what is causing the water masses in the model to be configured as they are.

To this end, it will be helpful to identify several of the major features of the T and S structure revealed in Fig. 6.

(i) What factors determine the temperature of the subthermocline water?

(ii) What factors affect the relative temperature of the deep water from major basin to basin?

(iii) What factors cause the meridional asymmetry in the temperature of the intermediate water of the Atlantic and Indian oceans?

It has been mentioned before, and the observed patterns of Fig. 6 confirm that salinity is much more highly structured in the ocean than is temperature. It may, therefore, be expected to be a more demanding test for simulation in a model than is temperature. The observed salinity configurations also vary much more from basin to basin than is the case with temperature. We will, therefore, discuss the response of each of the three model sectors, Atlantic, Indian and Pacific, individually and in turn.

(iv) *Atlantic sector.* What factors determine the salinity and positioning of the high salinity tongue from the north and the low salinity tongue overlying it from the south?

(v) *Indian sector.* What factors determine the salinity and positioning of the low salinity tongue from the south at intermediate depths, and the distinctive

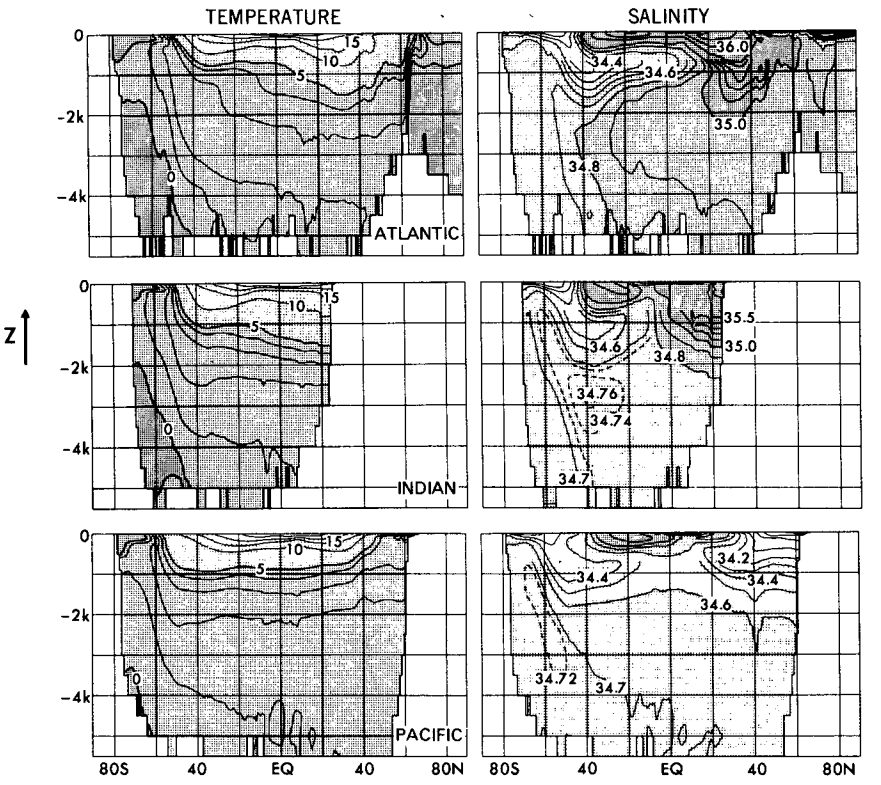

FIG. 6. Observed, long-term mean, zonally averaged T and S redrafted from Levitus (1982). Note that the contour interval for salinity in this figure is double that for subsequent figures depicting model results. Also, dashed contours represent a change in contour interval for this and subsequent figures.

maximum in salinity lying beneath it and well isolated from the southern boundary?

(vi) *Pacific sector.* What factors determine the salinity and positioning of the low salinity tongues from both the north and south at intermediate depths? What factors determine the distinctive north-to-south increase in salinity of the deep water, with a maximum reached north of the southern boundary?

a. Temperature of the subthermocline water

The temperature and salinity patterns of the solutions are presented in a series of three figures, Figs. 7–9, representing a progression through the four experiments for each of the three basins. The shape of the thermocline responds similarly for each of the three basins as we progress from Expt. 1 to Expt. 3. In agreement with the results discussed in section 3, the temperature below the thermocline, which is relatively low in the no-gap case of Expt. 1, increases markedly in each basin of Expt. 2 as the ACC isolates the extreme Southern Ocean, allowing less dense water from the north to make partial entry to the deep basins.

As we proceed to Expt. 3, the effect of wind gives the thermocline its familiar bowl shape in shallow midlatitudes, associated with the wind-driven gyres in each of the three basins. There is, however, an additional and even more important effect of the wind driving on the deep temperatures. As the amplitude of the ACC increases under the driving of the strong zonal winds in the Southern Ocean, the isolation of the extreme Southern Ocean increases, again due to the additional meridional density gradient needed across the current for geostrophic balance. This results in a further decline of density north of the ACC and a further deepening of the thermocline. Relative to the observed patterns of Fig. 6, the net effect of the changes from Expt. 1 to Expt. 3 has been to increase the subthermocline temperatures from too low to too high. Clearly, the model results indicate that the existence and amplitude of the ACC have a strong influence on the temperatures in the deep ocean. That they become too high in Expt. 3 may be due to the fact that the ACC in the model (96 Sv in Expt. 2 and 274 Sv in Expt. 3) becomes substantially stronger than the observational estimates, e.g., 123 Sv by Whitworth and Peterson (1985). Such an overestimate of the ACC by the model is most probably due to the absence of meridional topographic barriers (except for the Drake Passage sill) which are likely to extract energy from the stream in the real ocean.

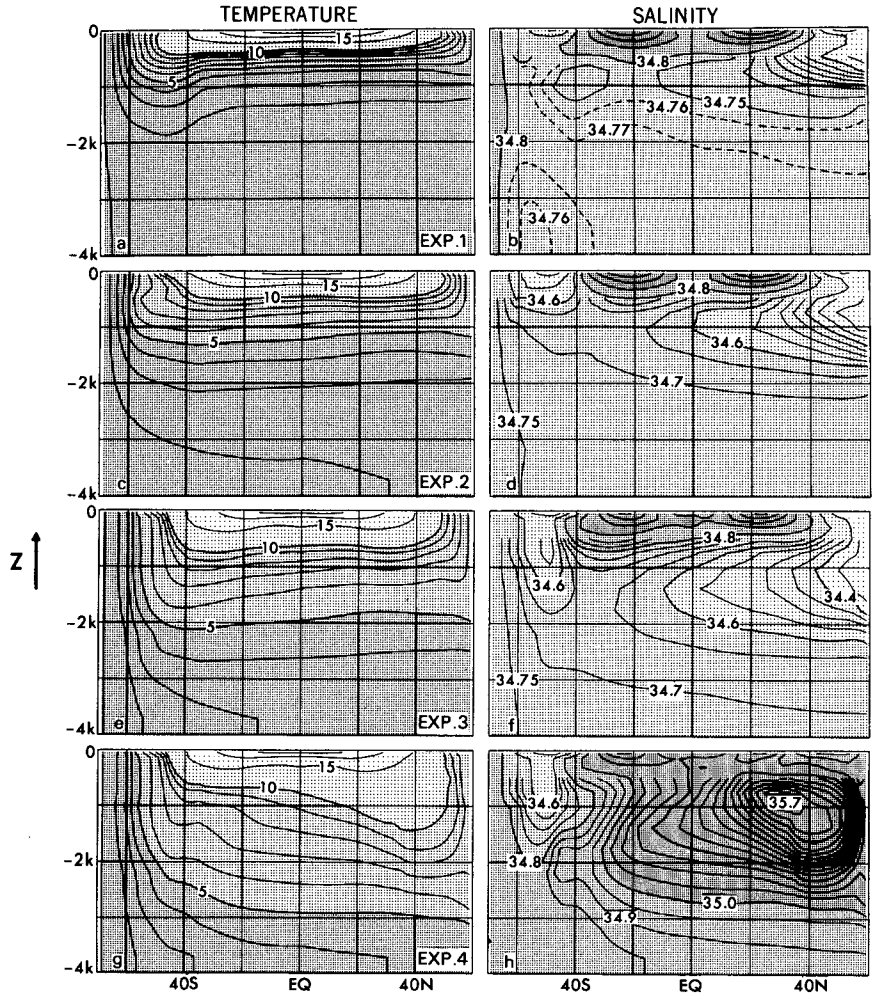

FIG. 7. Zonally averaged T and S for the Atlantic sector of the model, for each of the four experiments.

b. Relative deep water temperatures, basin-to-basin

The variation in deep water temperatures between basins observed in the model results is small compared to the global shifts noted above across the first three experiments. However, there is a subtle but interesting effect evident in the extreme southern deep ocean of the model solutions that compares favorably with the tendency in the observed patterns. A slight west-to-east increase in temperature occurs in this region as we pass from the Atlantic to the Pacific sectors. This gradient is present in Expt. 1 (using the presence or absence of the 1°C isotherm as a gauge), is reversed in Expt. 2, and, interestingly, is restored by the wind-driving of Expt. 3. The implication from this result is that the observed gradient in Fig. 6 in this region may be enhanced by wind-driving, although the effect in the model is not large. The subsequent analysis of circulation patterns in Part 2 of this study may shed more light on this mechanism.

c. Meridional asymmetry in the North Atlantic and Indian oceans

The greatest remaining difference in the major features of the observed temperature patterns of Fig. 6 and the model solutions is the meridionally asymmetric warming of the northern midlatitude intermediate waters in the Atlantic and Indian sectors. When a strong source of salinity is added in the North Atlantic in Expt. 4, such an effect is noted strongly in the model Atlantic. No such additional source of salt is added in the Indian sector, such as saline outflow from the Red Sea and Persian Gulf, and the disagreement with observations remains. The thermocline sag in the model is clearly related to the surface introduction of salt, and is presumably a result of the increased density of the water so produced.

d. Salinity of the Atlantic sector

The salinity configuration in the Atlantic sector of the model solutions evolves across the four experi-

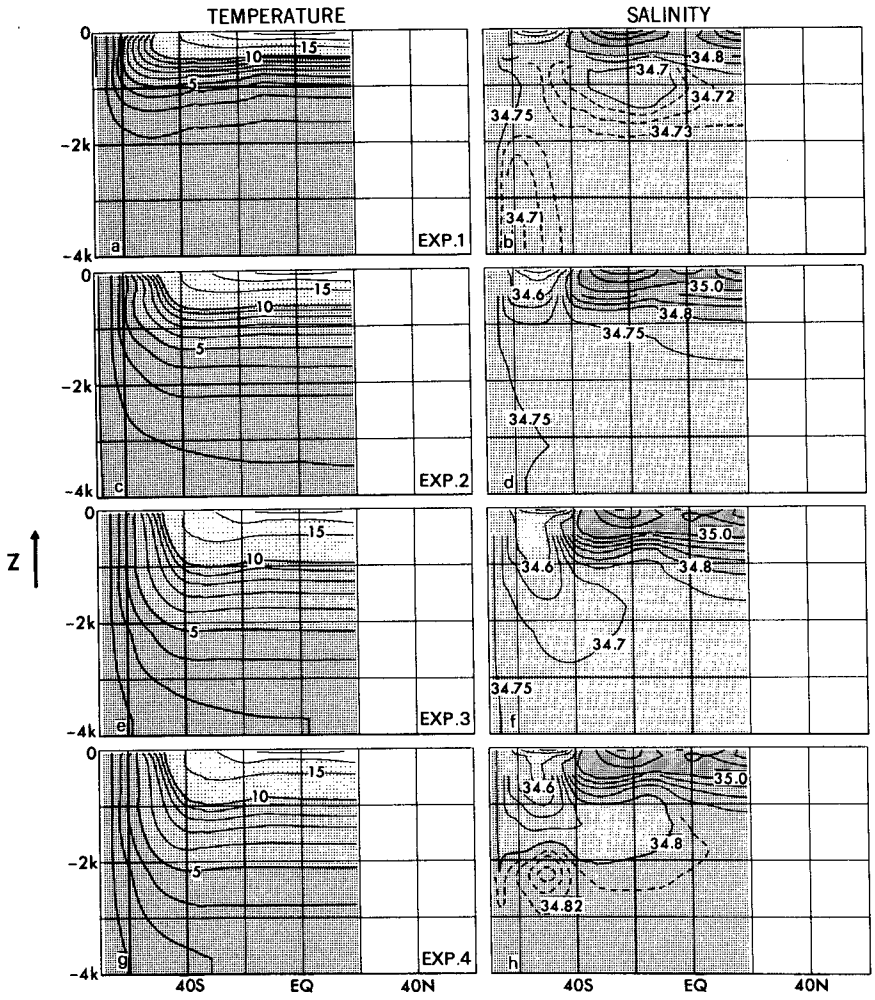

FIG. 8. As in Fig. 7 but for the Indian sector.

ments, from a pattern which is quite different from that seen in Fig. 6, to one which is similar. Since there is a freshwater source specified by S^* at the northern wall of the Atlantic in Expts. 1–3, the salinity signature of any intermediate or deep water formed there will be low for those three experiments. In agreement with the discussion of section 3, in the absence of an ACC to suppress Southern Ocean deep-water formation, the production of intermediate water along the northern wall in Expt. 1 is quite weak and shallow (Fig. 7b). Low salinity water derived from the minimum in S^* in the Southern Ocean is realized in two weak but distinct minima in this case, one located at 40°S and 1000 meter depth and the other at the bottom and near the southern wall. In both cases, the source of the minima is the Pacific basin (discussed later) which is made much fresher than the other basins by the closing of Drake Passage in this experiment. Since the freshwater in the Pacific basin cannot pass to the east directly into the Atlantic, it follows both a westward route north of Australia, through the Indian basin and south of Africa producing the shallower South Atlantic minimum, as well as a deeper westward route directly along the southern boundary, producing the minimum at the bottom.

As we progress through Expts. 2 and 3 (Figs. 7d, f), with the opening of the Drake Passage, both of these minima of eastern origin disappear and are replaced by a shallower minimum produced from the west. The effect of the strengthening ACC in isolating the extreme Southern Ocean is reflected in the ability of the low salinity tongue produced along the northern wall of the Atlantic sector to penetrate deeper and farther southward.

Finally, in Expt. 4 (Fig. 7h), in response to the introduction of a high salinity source in the North Atlantic, the signature of the deep water produced along the northern wall there switches from low to high salinity in agreement with observations. The additional density this change adds to the water mass enables it

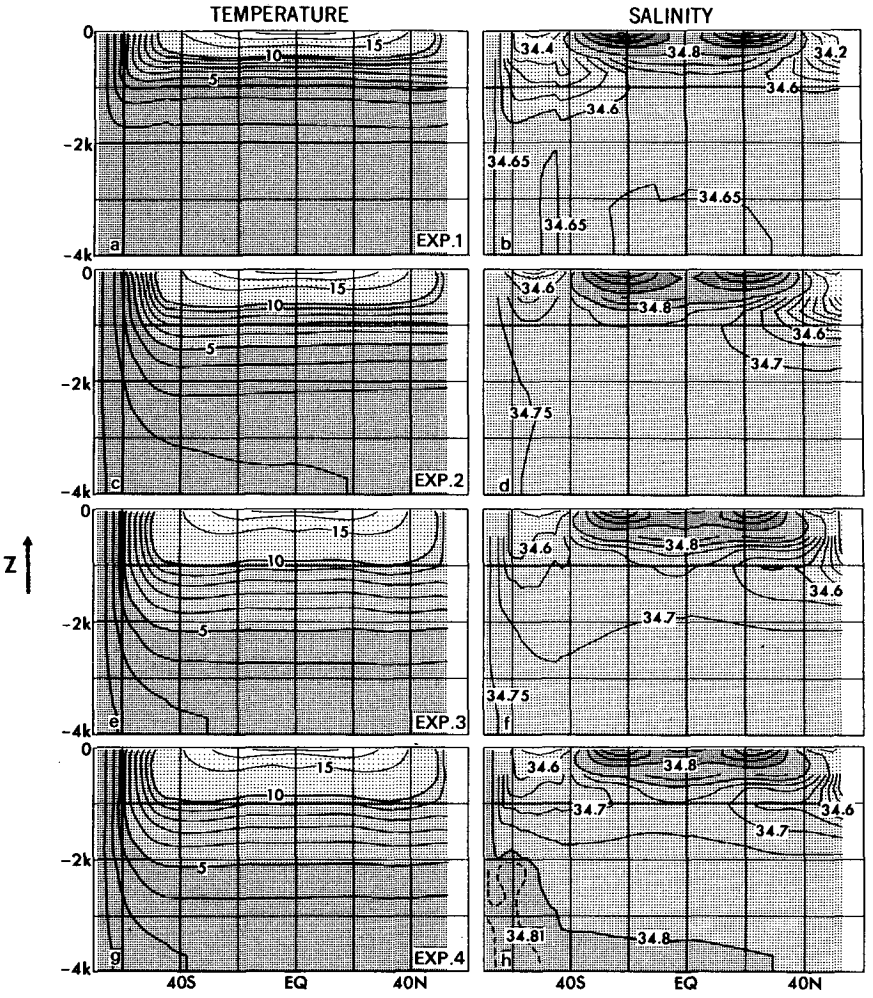

FIG. 9. As in Fig. 7 but for the Pacific sector.

to penetrate still farther in depth and to achieve greater southerly latitudes. The subsurface maximum in salinity in the northern Atlantic, not present in the observations, is presumably due to the less than realistic manner in which salt is introduced there, as described earlier. The fresh, intermediate water tongue from the south persists but does not penetrate northward above the northern source water to the extent in Fig. 6. This may be a case of just too little vertical resolution within the model to reproduce such a highly structured configuration, or may be a more substantial effect concerning the circulation more directly.

e. Salinity of the Indian sector

The salinity signature of the two westward flowing currents carrying freshwater from the Pacific basin described in Expt. 1 above are seen even more distinctly in Fig. 8b for the Indian sector. Again, these two minima are replaced in Expts. 2 and 3 by a minimum of shallower, western origin, and deepened by the wind driving effects. Finally, the introduction of high salinity water into the North Atlantic in Expt. 4 produces a deeper salinity maximum underlying the freshwater tongue. This final change in boundary conditions produces a salinity pattern for the Indian sector which agrees reasonably well, in terms of large-scale features, with the corresponding pattern in Fig. 6. The deepening of the halocline in the real northern Indian Ocean, absent in Fig. 8, is presumably produced by excess evaporation there. It has no counterpart in the simplified boundary conditions considered in these experiments.

f. Salinity of the Pacific sector

It was mentioned earlier that the Pacific sector, in Expt. 1, is very fresh relative to the other two basins. This large-scale zonal tilt in the halocline is produced primarily by the blockage of flow at Drake Passage in this experiment. Freshwater produced in southern latitudes by the surface boundary condition is carried

eastward by geostrophically induced flow at the surface across the entire southern ocean, converges upon the wall bounding the eastern pacific, and is forced to sink, filling the Pacific sector with water of relatively low salinity (Fig. 9b). When the Drake Passage is opened in Expt. 2, the induced vertical motion is greatly relieved in the southeast Pacific sector and the global zonal gradient across the southern deep ocean is reduced markedly.

Tongues of freshwater form and spread equatorward from both the northern and southern surface salinity minima imposed by S^*. As we proceed from Expt. 1 to Expt. 2, the tongue of southern origin recedes due to the reduction of wall-induced downwelling. However, just as in the Atlantic sector, the northern tongue advances due to its relatively greater ability to compete with deep-water production in the Southern Ocean, now more isolated by the presence of the ACC. For the same reason, both tongues advance in Expt. 3 as the ACC accelerates.

Finally, the remote effects of inserting additional salt in the North Atlantic are seen in Expt. 4 as a new deep maximum in salinity near, but still removed somewhat to the north of the southern boundary. Water of this higher salinity does not, however, fill the deep Pacific to the north. Without further analysis, it is impossible to say conclusively how the observed south-to-north gradient in deep salinity is maintained. A reasonable speculation may be that diapycnal mixing with the layer of low salinity water situated at intermediate depths to the north strikes a balance with northward transport of higher salinity southern deep water. In any case, once again the pattern of salinity from Expt. 4 possesses all of the large-scale features of the observed pattern for the Pacific in Fig. 6.

6. Water mass origins

Since all lateral and bottom boundaries in the model are specified to yield zero flux in T and S, the origin of the water masses observed in Figs. 7–9 must ultimately be the surface fluxes produced by T^* and S^*. How do the distributions adopted for these functions (Fig. 2) yield the patterns of Figs. 7–9? Direct analysis of the T and S patterns generally produces inconclusive results in addressing this question because there are multiple sources of warm, cold, fresh and salty water specified in T^*, S^*. This is, of course, a limiting factor in analyzing observed data from the real ocean as well. Just as natural and anthropogenic tracers have been used effectively as a tool in this type of analysis for the real ocean, theoretical tracers may also be included in the numerical model to assist in the analysis of its solutions.

The particular tracer used here (suggested by W. Broecker, private communication, 1988) is internally conserved, with sources and sinks specified only at the surface. It obeys the same equations used for T and S including the convective process produced by static instability. The function Tr* (the equivalent of T^*, S^* for temperature and salinity) is taken to be bimodal with the arbitrary values of one yielding a source for a particular grid box, and zero yielding a sink. A group of such tracers may be defined, each member of which has a specific, unique ocean surface area designated as its source region. When such a group is implemented in a model such as the present one, where quantities are formally conserved internally through advection, diffusion and convection (demonstrated in the model documentation cited earlier), they exhibit the following very useful property. If each grid box of the surface layer of the model is specified as a source (Tr* = 1) of one and only one of the group of tracers, and therefore a sink of all the other tracers in the group, and a steady, well-converged solution is obtained, then at any internal gridbox of the model, the sum of concentrations of all tracers in the group will be one. This means that, for any arbitrary subvolume of the model domain, a complete census may be obtained yielding the percentage of water within that subvolume deriving from the various surface source areas associated with the various member tracers in the group.

Formulating such a group of tracers for the purpose of analyzing the solutions obtained here is somewhat arbitrary. A large group would afford more conclusive and detailed results but would be more costly in computation and more complex to analyze. A group of five tracers has been chosen here. Their source regions, shown at the top of Fig. 10, cover the surface of the

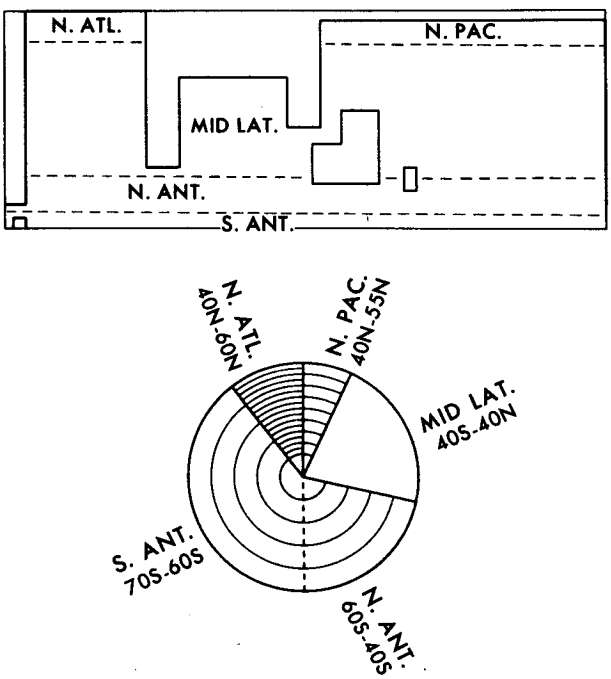

FIG. 10. Source areas for the five tracers (top), and key to the pie-diagrams used to show census of water mass origins (bottom).

model in a manner which corresponds to the various anticipated water mass formation areas. A South Antarctic tracer is specified from the southern wall to 60°S (center of Drake Passage) for all longitudes; a North Antarctic tracer from 60° to 40°S for all longitudes; a midlatitude tracer from 40°S to 40°N for all longitudes; a North Atlantic tracer from 40°N to the northern wall in the Atlantic only; a North Pacific tracer from 40°N to the northern wall in the Pacific only. Water deriving from these five regions will henceforth be referenced as "South Antarctic water," "North Atlantic water," etc.

A pie-diagram is used in subsequent figures to represent the census of water mass origin for various subvolumes of the model domain. A key to the diagrams is given in Fig. 10 where each of the five surface regions are represented by wedges filled with shading of differing density. The southern and northern components of the Antarctic region are separated by a dashed line, with the southern component always to the left. Where a wedge represents more than 3% of the total water mass, the percentage is given directly outside of the wedge in the subsequent figures.

Before proceeding to analyze the water mass origins basin-by-basin, we will present a broader view, describing the census for the entire integrated World Ocean. For this purpose, we have divided the subthermocline ocean into two members vertically. Identified as "intermediate water" is that water residing between 876 and 2406 meters depth (levels 6–9 of the model.) "Deep water" is defined as that lying between 2406 meters and the bottom at 4000 meters (levels 10–12 of the model.) Note that 2406 meters corresponds to the depth of the Drake Passage in Expts. 2–4. Figure 11 contains pie-diagrams illustrating the water mass origin census for each of the four experiments and for the two depth ranges covering the integrated World Ocean.

The dominating influence of water of extreme southern origin in Expt. 1 is once again seen in this census. Fully 87% of the deep water and 81% of the intermediate water of the total ocean are formed in the South Antarctic region, with the remainder deriving mostly from the North Antarctic. When the Drake Passage is opened in Expt. 2, the influence of the extreme Southern Ocean on the intermediate water falls considerably, with midlatitude and northern sources increasing in influence. The same exchange occurs in the deep water, although not as strongly. When wind is added in Expt. 3, however, the resultant strengthening of the ACC brings about a deepening of the isolation of the South Antarctic and its influence falls by roughly 20% in both intermediate and deep sectors. In this case, however, about half of the water replacing it comes from the North Antarctic with the remainder deriving from farther north.

Finally, when surface salinity is increased in the North Atlantic in Expt. 4, the influence of the North Atlantic water nearly doubles in the intermediate sector worldwide and triples in the deep sector to 16% of the total. This results in yet another reduction in influence of the South Antarctic water as well as an accompanying reduction of both North Antarctic and North Pacific water. Midlatitude water shows a slight gain in influence in this case.

The influence of waters formed in midlatitudes upon the deep water in the ocean is often assumed to be small or even insignificant. However, Broecker et al. (1985), considering initial phosphate concentrations, conclude that intermediate waters in the tropical Indian and Pacific, while mainly of Antarctic origin, contain roughly 10% warm upper water. This water is, in turn, a significant component in the formation of the deep waters of these basins. The results shown in the pie-diagrams of Fig. 11 indicate that the influence of water of midlatitude origin upon the deep water is also significant in the model solutions. In Expt. 4, fully 10% of the deep water of the total World Ocean in the model is derived from midlatitudes, presumably through vertical diffusive processes. The value of the coefficient of vertical diffusion used will have a strong influence upon the presence of midlatitude water in the deep ocean, and further experimentation should be carried out to investigate this question. However, the magnitude adopted here, 0.5 $cm^2\ s^{-1}$, is close to that estimated for the thermocline region and well below that typically estimated for the deeper ocean. The results above may, therefore, be expected to be a reasonable estimate of the influence of midlatitude water upon the deep ocean.

We will now proceed with a more detailed, basin-by-basin analysis of the data presented above. Figures 12–14 illustrate, for the zonally averaged Atlantic, Indian and Pacific basins of the model respectively, the relative influence of the surface region represented by each tracer, showing percentage of the local water de-

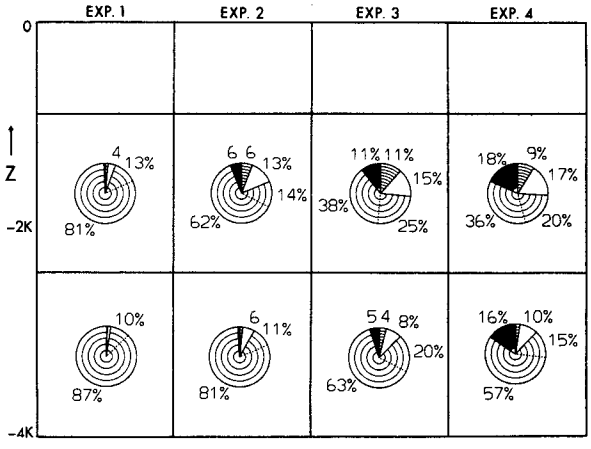

FIG. 11. Census of water mass origins for the integrated World Ocean in each of the four experiments for intermediate water (876–2406 m), and deep water (2406–4000 m).

riving from each region. The patterns associated with the midlatitude source, shaped much like the temperature patterns of Figs. 7–9, are generally less variable than the other four and therefore are not shown. They compose the complementary percentage not represented in Figs. 12–14. The influence from the Northern Atlantic and Pacific regions are combined in the third column in each figure, with dashed lines representing the North Pacific component in the first figure and the North Atlantic component in the subsequent two figures.

Pie-diagrams are provided in the fourth column representing the subvolumes of each basin described by the boxes in which they reside. These boxes extend from the southern wall to the equator and the equator to the northern wall of each basin. Vertically, they are partitioned into the same intermediate and deep sectors which were used in Fig. 11. These four boxes will henceforth be referenced by the terms "northern" or "southern," and "intermediate" or "deep."

a. Water mass origins in the Atlantic sector

As expected, in Expt. 1, water of South Antarctic origin dominates the Atlantic sector of the model shown in Fig. 12. The influence of North Atlantic water is seen, in this case, to be confined largely to shallow regions of the North Atlantic. When the Drake Passage is opened in Expt. 2, the influence of the South Antarctic water is reduced considerably, particularly at intermediate depths where each of the other water types except North Pacific show significant increases in influence. A similar shift takes place in the deep water, although not as large.

Upon adding wind in Expt. 3, further advances are made by waters deriving from surface regions north of the ACC. The influence of the North Antarctic water deepens considerably. Also, the North Atlantic water begins to dominate the intermediate depths of the North Atlantic and increases its influence within the deep water. A trace of North Pacific water appears at shallow depths in the South Atlantic as well. When extra salt is inserted into the North Atlantic in Expt. 4, the influence of the North Atlantic water is again increased significantly. Not only does its concentration deepen north of the equator, but, more importantly, it advances strongly to the south. In so doing, it forms a wedge between the North and South Antarctic water, causing the former to recede even further and driving the latter to more shallow depths.

The influence of waters formed in midlatitudes upon the deep water in the three individual basins in Expt. 4 does not vary greatly from basin-to-basin. In each, it is roughly equal the 10% of the worldwide distribution.

b. Water mass origins in the Indian sector

Water of South Antarctic origin dominates the intermediate and deep waters of the Indian sector (Fig. 13) in Expt. 1 much as it does in the Atlantic. A trace of North Pacific water enters the Indian basin north of Australia in this case as well. With the opening of Drake Passage and the addition of wind driving, the influence of South Antarctic water diminishes considerably. Water of North Antarctic origin deepens and forms a lens to the north at intermediate depths. As the influence of North Pacific water increases within the Pacific sector (discussed next), it also invades the Indian sector more strongly, positioning above the lens of intermediate North Antarctic water from the south.

In Expt. 4 the influence of the North Atlantic water is seen for the first time in the Indian sector as a lens positioned between the primary influence of the South and North Antarctic waters. The latter is, in turn, wedged between the lenses of North Atlantic and North Pacific waters forming a rather intricate sandwich of different water types.

c. Water mass origins in the Pacific sector

The patterns for Expt. 1 in Fig. 14 for the Pacific sector are similar to the corresponding ones for the Atlantic sector, with water of South Antarctic origin once again playing the dominant role. The influence of North Antarctic water is deeper in the Pacific in this case, however, because of the wall-induced downwelling along the eastern boundary which was discussed earlier. In Expt. 2, its influence is diminished by opening the Drake Passage, thereby reducing the wall-induced vertical motion. The influence of North Pacific water increases in Expt. 2, again due to the effect of the ACC in impeding the northward penetration of the more dense South Antarctic water. The introduction of wind driving in Expt. 3 increases this effect, allowing both the North Antarctic and North Pacific lenses to advance. Note however, that the relative magnitude of influence of the water of North Pacific origin within the Pacific is not as great as that of North Atlantic water in the Atlantic, even before extra salt is added to the North Atlantic in Expt. 4. This may be explained by the higher latitude of the northern boundary of the Atlantic (60° vs. 55°), causing its density at the wall to be, from the boundary conditions of Fig. 2, slightly higher.

Just as in the Indian sector, the influence of the North Atlantic water is seen with significance for the first time in the Pacific basin in Expt. 4. Although its presence is only about half as great as in the Indian sector, at 9% it still accounts for a significant component of the deep water in the Pacific, with a maximum occurring near, but distinctly north of the southern boundary.

7. Regimes of water mass exchange between experiments

As stated earlier, the goal of the present study is not primarily to simulate the real ocean so much as to study the reaction of the model to the three changes in boundary condition imposed in the four experi-

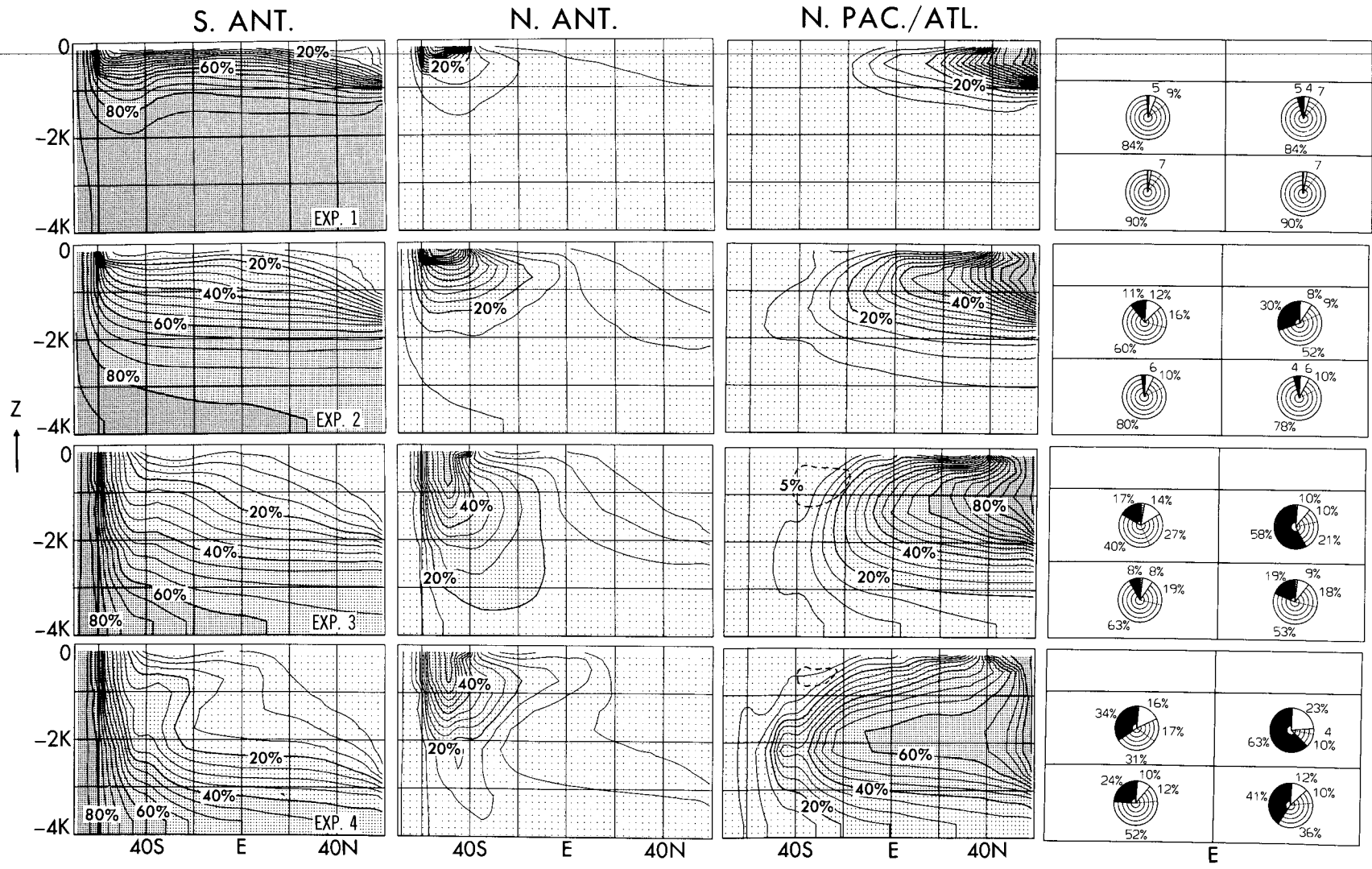

FIG. 12. Composition of water masses by region of surface formation for the Atlantic sector of the model. Solid lines in column 3 represent water of North Atlantic origin, dashed lines designate North Pacific origin. Pie-diagrams cover the volume of the box in which they are positioned.

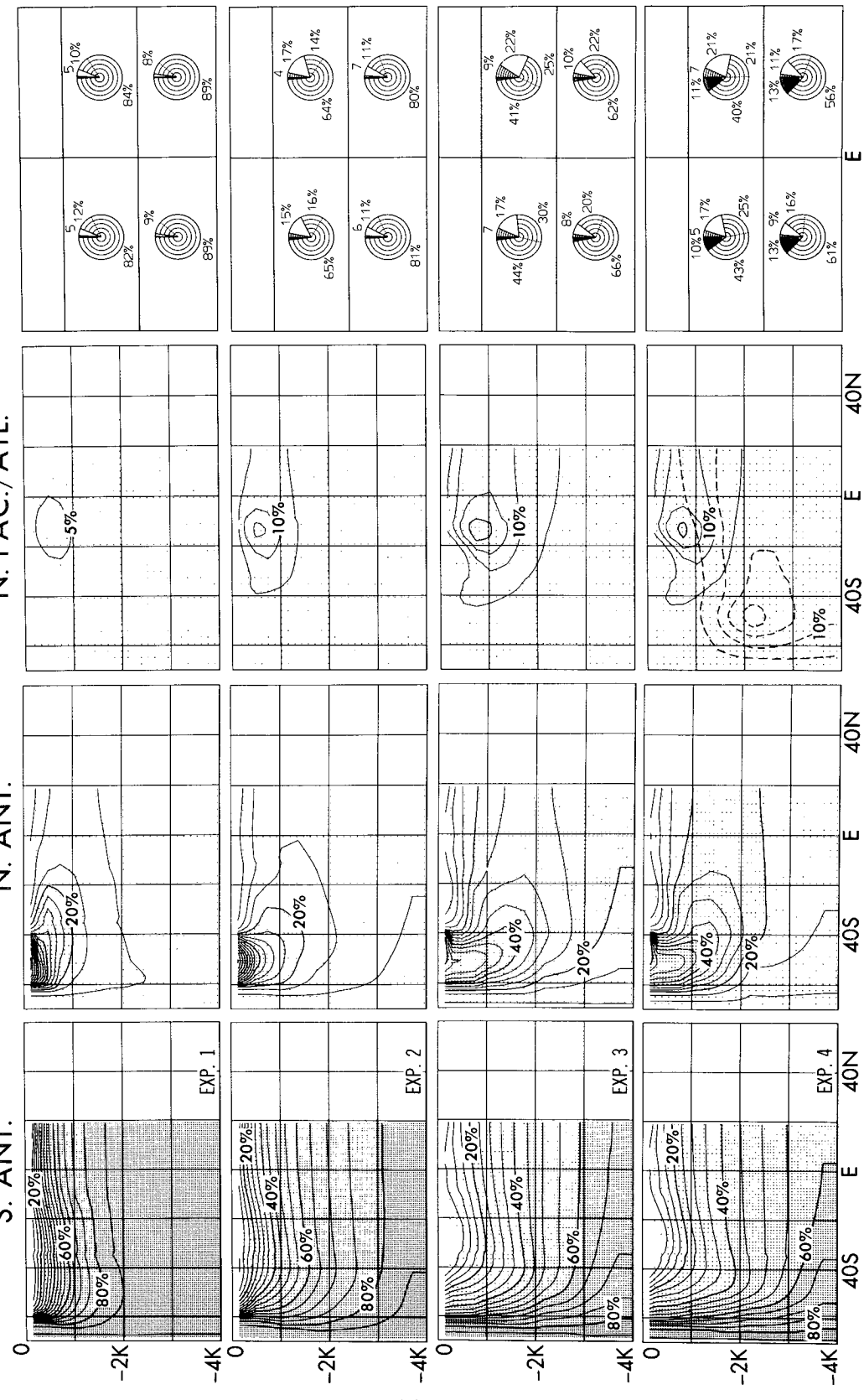

FIG. 13. As in Fig. 12 but for the Indian sector of the model. Solid lines in column 3 represent water of North Pacific origin, dashed lines designate North Atlantic origin.

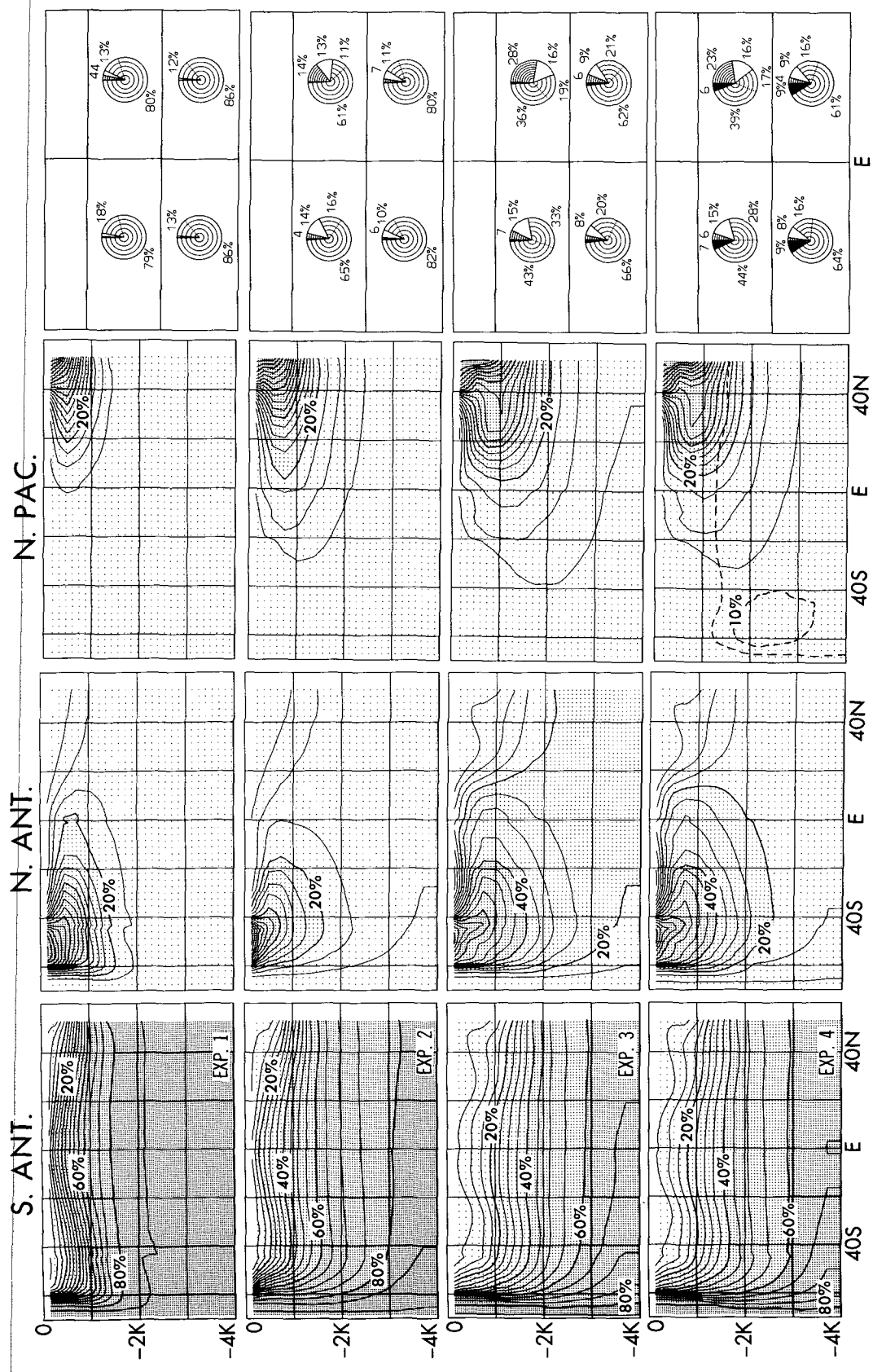

FIG. 14. As in Fig. 12 but for the Pacific sector of the model. Solid lines in column 3 represent water of North Pacific origin, dashed lines designate North Atlantic origin.

ments. An additional analysis has been carried out on the tracer data to evaluate more directly the changes in water mass origins arising from the three alterations in boundary condition: inclusion of an ACC by opening the Drake Passage, addition of wind driving, and surface production of a saline North Atlantic Deep Water (NADW). For each of the three experimental pairs, this analysis seeks to identify a dominant regime of exchange between any two of the water masses. Among the five water masses identified by the tracer data, there are 20 possible such pairs of advancing and receding water. These regimes are listed in Fig. 15 and identified in the left-hand column with a single letter.

For each grid box in latitude and depth, for each of the three zonally averaged sectors of the model, a particular exchange regime is said to dominate if it alone accounts for at least 50% of the total exchange of advancing and receding waters at that point. The results are shown in Fig. 16 for each sector and each change in boundary condition. If a dominant exchange regime exists for a given grid box, it is identified with a letter corresponding to the regime listed in Fig. 15. The absence of a letter indicates that no such dominant regime exists. The total percentage of water which is replaced by all exchanges is indicated by contours of 10% each.

REGIME	ADVANCING WATER	RECEDING WATER
A	N. ATL.	N. PAC.
B	N. ATL.	MID LAT.
C	N. ATL.	N. ANT.
D	N. ATL.	S. ANT.
E	N. PAC.	N. ATL.
F	N. PAC.	MID LAT.
G	N. PAC.	N. ANT.
H	N. PAC.	S. ANT.
I	MID LAT.	N. ATL.
J	MID LAT.	N. PAC.
K	MID LAT.	N. ANT.
L	MID LAT.	S. ANT.
M	N. ANT.	N. ATL.
N	N. ANT.	N. PAC.
O	N. ANT.	MID LAT.
P	N. ANT.	S. ANT.
Q	S. ANT.	N. ATL.
R	S. ANT.	N. PAC.
S	S. ANT.	MID LAT.
T	S. ANT.	N. ANT.

FIG. 15. Regimes of water mass exchange.

a. Water mass exchanges due to the opening of Drake Passage

The dominant exchange regimes occurring when the Drake Passage is opened are shown for each of the three sectors of the model in the left hand panels of Fig. 16. In the North Atlantic, consistent with the earlier discussion, replacement of South Antarctic water by North Atlantic water (D) dominates a strong total exchange of water at intermediate depths. Further south, the dominant exchange is North Antarctic water replacing South Antarctic water (P). In the Indian basin, the receding South Antarctic water is replaced primarily by midlatitude water (L) penetrating downward into intermediate depths. Although this same exchange occurs in the deep water, its magnitude is quite small. A similar exchange is seen in the Pacific basin, although advancing North Pacific water (H) is dominant at intermediate depths in the north. A strong exchange takes place near the surface at the latitude of Drake Passage, dominated by an exchange of North Antarctic water by South Antarctic water (T). This is an effect of the suspension of wall-induced downwelling when the passage is opened, as discussed earlier.

b. Water mass exchanges due to wind driving

The center panels of Fig. 16 show the effects of wind driving on the water mass origins. Again, the exchanges are dominated by recession of the South Antarctic water. However, they are somewhat more significant in the deep basins than those due to the opening of the Drake Passage alone. In the North Atlantic, once again the dominant regime is the replacement of South Antarctic water by North Atlantic water, although at a greater depth and extending with appreciable amplitude to the bottom. In the South Atlantic, a somewhat weaker, but still significant replacement of South Antarctic water is accomplished primarily by advancing North Antarctic water (P). This exchange regime dominates the entire subthermocline region of both the Indian and Pacific basins, with the exception of a small region of the intermediate North Pacific where advancing North Pacific water prevails.

c. Water mass exchanges due to saline NADW

The third column of Fig. 16 depicts the water mass exchanges resulting from the introduction of additional salt through the surface of the North Atlantic. Further replacement of South Antarctic water by North Atlantic water takes place in the Atlantic at still greater depths, and at more southerly latitudes, indicating the improved ability of the NADW to penetrate southward

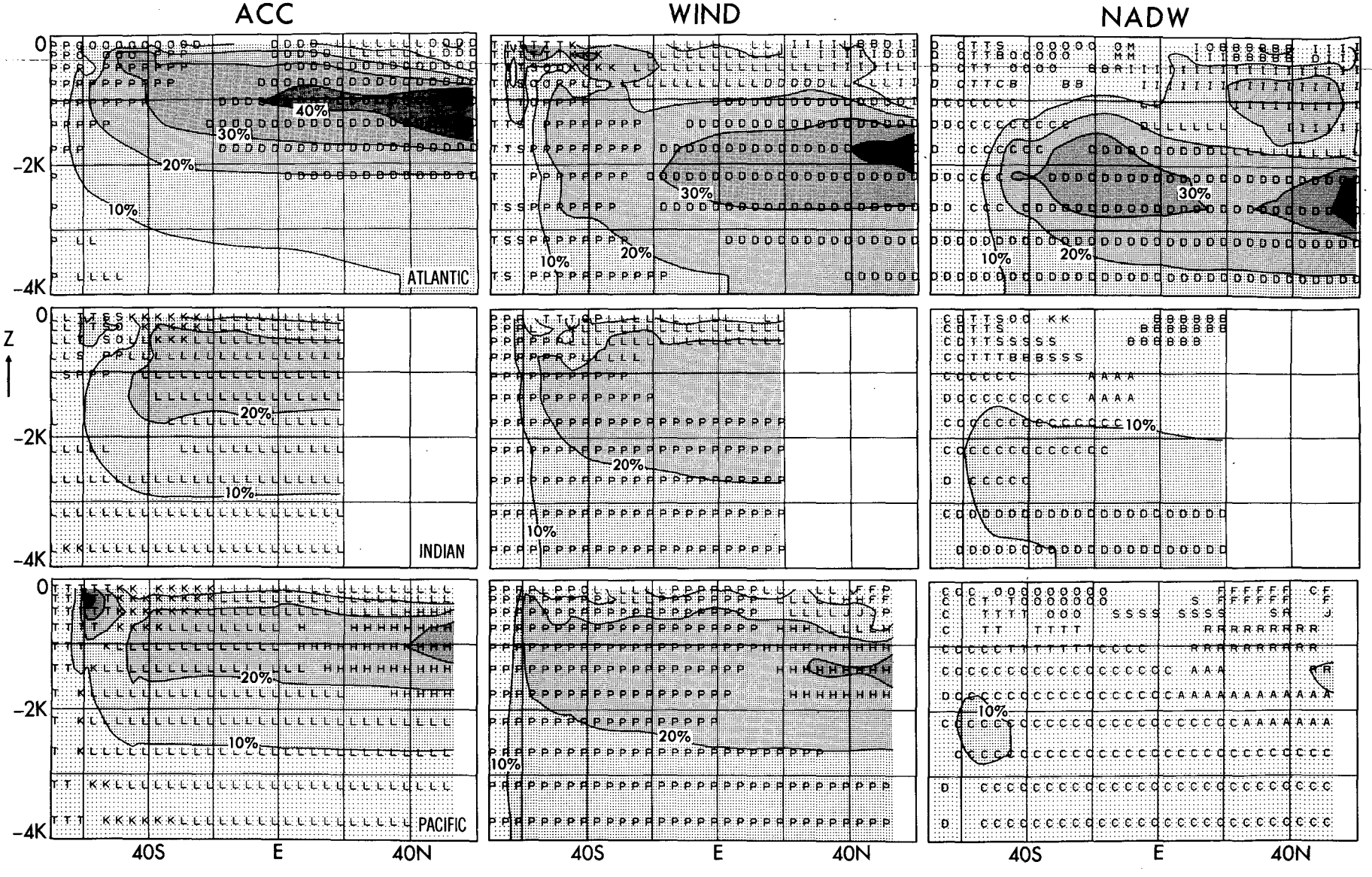

FIG. 16. Zonally averaged water mass exchanges for the three basins of the model and for the three changes in boundary condition. Letters designate dominant regimes listed in Fig. 15. Contours represent percentage of water replaced by all exchanges.

at its new, higher salinity. In the higher latitude South Atlantic, NADW replaces North Antarctic water (C) primarily. Replacing the NADW at its previous, shallower depth in the north is water of midlatitude origin (I). In the Indian basin, the most significant exchange occurs in the deeper ocean where NADW replaces South Antarctic water near the bottom, and North Antarctic water above. The exchanges in the Pacific are small but still dominated by the advancing NADW. In the deep ocean, North Antarctic water is being replaced primarily. At intermediate depths in the North Pacific, the North Pacific water is forced into retreat by NADW from below (A) and South Antarctic water from above (R).

8. Summary and conclusions

A primitive equation numerical model, using a simple turbulence closure scheme and idealized topography, is used here to study the major water mass properties of the World Ocean as revealed in zonally averaged patterns of temperature and salinity for the three primary basins. An initial experiment (Expt. 1) is conducted using only thermohaline forcing and allowing for no cyclic flow around the Southern Ocean. The evolution of the water mass configurations are then studied in response to the incorporation of three primary extensions to the model boundary conditions: opening of Drake Passage (Expt. 2), addition of wind driving (Expt. 3), and increase of salinity at the surface of the North Atlantic (Expt. 4). Idealized tracers are used to study the surface origins of the water masses produced in the model.

a. Solution from the initial experiment

The tracer patterns (Figs. 12–14) indicate that, in Expt. 1, water originating near the southern wall of the model dominates both the intermediate and deep sectors of the entire World Ocean. Both the intermediate and deep regions of the model are composed of more than 80% water formed in the extreme Southern Ocean. This highly dense water tends to block the vertical penetration of waters formed at more northerly latitudes and results in a virtual homogenization of the intermediate and deep ocean. Even in the presence of this strong driving from the south, however, several features of the observed patterns (Fig. 6) are reproduced (Figs. 7–9) by these highly idealized boundary conditions. A general thermocline is present, although far too shallow, and a reasonable halocline is produced in lower latitudes above 500 meters depth.

Below this level, however, the salinity patterns deviate markedly from those observed. Occurrence of low salinity intermediate water in the Southern Ocean is limited to the Pacific basin and only small, shallow tongues of fresh water penetrate southward from the northern walls of the Atlantic and Pacific. The reverse halocline found at depth in many parts of the real ocean is absent.

b. Effect of opening Drake Passage

Opening the Drake Passage and allowing for a cyclic flow around the Southern Ocean has a profound effect on all of the patterns in the intermediate and deep ocean. In accordance with the findings of section 3, the presence of an Antarctic Circumpolar Current serves to partially isolate the extreme Southern Ocean, allowing waters created at lower latitudes and northern latitudes to penetrate farther vertically and thereby participate more vigorously in the formation of intermediate and deep waters. The tracer data reveal this effect as waters of North Atlantic, North Pacific, and midlatitude origin all make advances, mostly replacing water of extreme southern origin.

The resultant T and S patterns become more realistic in this case. The general thermocline deepens in all sectors of the model, and tongues of intermediate water penetrate farther, both vertically and southward from the northern walls of the Atlantic and Pacific. In the Southern Ocean, fresh intermediate water, formerly limited to the region of downwelling along the closed eastern wall of the South Pacific, now is able to spread worldwide through the opening of the Drake Passage. This produces the beginnings of somewhat more realistic lenses of such water in the Atlantic and Indian sectors.

c. Effect of adding wind driving

When a simple zonal wind stress based upon observations from the real World Ocean is applied to the previous model, the solution undergoes some additional fundamental changes. Once again, the most basic response is the resultant increase in the magnitude of the Southern Ocean throughflow. As the ACC increases under the wind driving, it serves to further isolate the extreme Southern Ocean. The tracer data, however, indicate that water of North Antarctic origin (formed at the surface just to the north of the ACC) plays a much more significant role in replacing the receding South Antarctic water in this case than the previous one in which the Drake Passage was opened. This results in a significant advancement of the region of influence of the North Antarctic water, both vertically and northward in each of the three sectors of the model World Ocean. The intermediate lenses emanating from the northern walls of the Atlantic and Pacific also make advances in this case.

The response of the temperature and salinity patterns to the wind driving is predictable from the tracer responses. As water of extreme southern origin recedes and is replaced by waters of lower latitude origins, the thermocline thickens even more and the temperature of the deep and intermediate waters of the World Ocean increase on a broad scale. The intermediate fresh water tongues emanating from the North Antarctic region deepen significantly to come into better agreement with

observations in each of the three basins. At the same time, the tongues of fresh, intermediate water originating from the northern walls of the Atlantic and Pacific advance to combine with those from the south to form a continuous wedge of fresh water lying below the more saline surface waters. Although this pattern is not realistic for the Atlantic due to the low salinity imposed upon the northern wall there by the boundary condition, it is similar to the observed patterns in the Pacific.

d. Effect of increasing surface salinity in the North Atlantic

Providing higher salinity to the waters formed in the northern regions of the North Atlantic through the surface boundary condition produces an important additional movement of the solution toward the observed patterns of Fig. 6, particularly with respect to salinity in the deep ocean. It is interesting to note that recent work (Broecker et al. 1985; Manabe and Stouffer 1988) suggests that the resulting response of the model may have strong implications for the transition between ice-age and present day oceanic states. The tracer patterns in the Atlantic indicate that the additional density acquired by the North Atlantic water enables it to penetrate farther, both vertically and to the south. In so doing, it wedges between the waters of North and South Antarctic origin in the South Atlantic, pushing the former above it and the latter below it. The resulting salinity patterns in this region become much more like those observed, possessing the well-known saline tongue of NADW at mid-depths, overlain by a freshwater lens of North Antarctic origin.

The tracer patterns for the Indian and Pacific basins indicate that the influence of the North Atlantic water extends right across the Southern Ocean, proceeding northward into those basins to become a significant component of their deep water as well. As a result, a well-defined salinity maximum arises in the southern Indian and Pacific basins, isolated from the southern wall and underlying the intermediate freshwater lenses there. This signature is directly attributable to the eastward flow of saline water originating in the North Atlantic and is clearly evident in the patterns of observed data.

Farther north in these basins, the intrusion of the saline water produces the observed reverse halocline in the deep water as well. In the Pacific basin, the observed south-to-north decrease of salinity in the deep water appears to be accomplished by a balance between northward advecting saline water and vertically diffusing water from the wedge of freshwater lying above. This assertion remains speculative, however. The exact manner in which the various end member source waters considered here combine to form the deep waters cannot be established by considering the water mass configurations alone. Broecker et al. (1985) suggest that Antarctic Bottom Water and North Atlantic Deep Water combine with water flowing out of the Indian and Pacific oceans at mid-depth to form the Antarctic Common Water from which much of the deep water is derived. Analysis of the large-scale circulation regimes of the solutions, presented in part 2 of this study, will go much further in determining how these combined water masses are formed in the model.

Acknowledgments. The author would like to thank K. Bryan and J. R. Toggweiler for helpful discussions concerning the analysis and interpretation of the experimental results. Also, thanks to W. Broecker who suggested the use of the passive tracers.

REFERENCES

Bolin, B., and H. Stommel, 1961: On the abyssal circulation of the World Ocean, 4, Origin and rate of circulation of deep ocean water as determined with the aid of tracers. *Deep-Sea Res.*, **8,** 95–110.

Broecker, W. S., D. M. Peteer and D. Rind, 1985: Does the ocean–atmosphere system have more than one stable mode of operation? *Nature,* **315,** 21–26.

——, T. Takahashi and T. Takahashi, 1985: Sources and flow patterns of deep-ocean waters as deduced from potential temperature, salinity, and initial phosphate concentration. *J. Geophys. Res.*, **90,** 6925–6939.

Bryan, F., 1986: High-latitude salinity effects and interhemispheric thermohaline circulations. *Nature,* **323,** 301–304.

Bryan, K., 1969: A numerical method for the study of the circulation of the World Ocean. *J. Comput. Phys.*, **4,** 347–376.

——, 1979: Models of the World Ocean. *Dyn. Atmos. Oceans,* **3,** 327–338.

——, 1984: Accelerating the convergence to equilibrium of ocean-climate models. *J. Phys. Oceanogr.*, **14,** 666–673.

——, and M. D. Cox, 1972: An approximate equation of state for numerical models of ocean circulation. *J. Phys. Oceanogr.*, **2,** 510–514.

Cox., M. D., 1984: A primitive equation, 3-dimensional model of the ocean. GFDL Ocean Group Tech. Rep. No. 1, 143 pp.

Gill, A. E., and K. Bryan, 1971: Effects of geometry on the circulation of a three-dimensional southern hemisphere ocean model. *Deep-Sea Res.*, **18,** 685–721.

Gordon, A. L., 1986: Interocean exchange of thermocline water. *J. Geophys. Res.*, **91,** 5037–5046.

Kuo, H. H., and G. Veronis, 1973: The use of oxygen as a test for an abyssal circulation model. *Deep-Sea Res.*, **20,** 871–888.

Levitus, S., 1982: Climatological Atlas of the World Ocean. NOAA Prof. Pap. 13, 1093–1104.

Manabe, S., and R. J. Stouffer, 1988: Two stable equilibria of a coupled ocean-atmosphere model. *J. Climate,* **1,** 841–866.

Reid, J., and R. Lynn, 1971: On the influence of the Norwegian-Greenland and Weddell Seas upon the bottom waters of the Indian and Pacific oceans. *Deep-Sea Res.*, **18,** 1063–1088.

Stommel, H., and A. B. Arons, 1960: On the abyssal circulation of the world ocean—I: Stationary planetary flow patterns on a sphere. *Deep-Sea Res.*, **6,** 140–154.

Toggweiler, J. R., K. Dixon and K. Bryan, 1989: Simulations of radiocarbon in a coarse-resolution World Ocean model I: Steady state, prebomb distributions. *J. Geophys. Res.*, **94,** C8217–8242.

Warren, B. A., 1981: Deep circulation of the World Ocean. *Evolution of Physical Oceanography,* B. A. Warren and C. Wunsch, Eds., MIT Press, 6–41.

Whitworth, T., III, and R. G. Peterson, 1985: Volume transport of the Antarctic Circumpolar Current from bottom pressure measurements. *J. Phys. Oceanogr.*, **15,** 810–816.

Worthington, L. V., 1981: The water masses of the World Ocean: Some results of a fine-scale census. *Evolution of Physical Oceanography,* B. A. Warren and C. Wunsch, Eds., MIT Press, 42–69.